Available online at www.sciencedirect.com
ScienceDirect
Physica D 223 (2006) 270–275
PHYSICA D
www.elsevier.com/locate/physd

Synchronization threshold in coupled logistic map lattices

C. Anteneodo[a,*], A.M. Batista[b], R.L. Viana[c]

[a] Departamento de Física, Pontifícia Universidade Católica do Rio de Janeiro, Caixa Postal 38071, 22452-970 RJ, Rio de Janeiro, Brazil
[b] Departamento de Matemática e Estatística, Universidade Estadual de Ponta Grossa, 84030-900 PR, Ponta Grossa, Brazil
[c] Departamento de Física, Universidade Federal do Paraná, Caixa Postal 19081, 81531-990 PR, Curitiba, Brazil

Received 20 January 2006; received in revised form 27 August 2006; accepted 5 October 2006
Available online 19 October 2006
Communicated by A. Doelman

Abstract

We consider regular lattices of coupled chaotic maps whose local dynamics is ruled by the logistic map $x \mapsto 4x(1-x)$, a usual paradigm of chaotic systems. Through finite-time exponents, we scrutinize the lattice dynamics in the vicinity of the threshold of complete synchronization. We connect dynamical features such as relaxation to the coherent state and intermittency with the statistics of finite-time exponents, focusing on the implications of the particular statistics related to the logistic map. Although numerical examples are given for lattice couplings decaying with distance as a power law, our results are expected to be valid for a wider class of schemes coupling logistic maps.

Keywords: Coupled map lattices; Synchronization; Intermittency

1. Introduction

Coupled map lattices (CMLs) have been intensively investigated since the early 80's as models to understand many spatiotemporal phenomena observed in extended systems [1]. Usual prototypes of CMLs are periodic chains of N identical one-dimensional chaotic maps $x \mapsto f(x)$ with symmetric (diffusive) distance-dependent interactions like in

$$x_{t+1}^{(i)} = (1-\varepsilon) f(x_t^{(i)}) + \frac{\varepsilon}{\eta} \sum_{r=1}^{N'} B(r) \times \left(f(x_t^{(i-r)}) + f(x_t^{(i+r)}) \right), \quad (1)$$

where $x_t^{(i)}$ represents the state variable for site i at discrete time t, $\varepsilon \geq 0$ is the coupling constant, $\eta = 2\sum_{r=1}^{N'} B(r)$ is a normalization factor, being $N' = (N-1)/2$ when N is odd, and $B(r)$ is in principle an arbitrary function of lattice distance r. Specially relevant cases correspond to algebraically decaying interactions, namely, $B(r) = 1/r^{\alpha}$, with $0 \leq \alpha$ [2,3], and to uniform interactions with a cut-off distance ρ (that is, $B(r)$ constant for $r \leq \rho$ and null otherwise), with $1 \leq \rho \leq N'$ [4]. These regular couplings allow us to model and investigate the effect of the range of interactions in the collective behavior of the lattice. Both cases include, as particular ones, the well known nearest-first-neighbor (for infinite α and $\rho = 1$, respectively) and global couplings (for $\alpha = 0$ and $\rho = N'$, respectively).

One of the interesting phenomena that CMLs display is synchronization and, in particular, amongst the various kinds of coherent behavior, *complete synchronization* [5]. It occurs when the dynamical variables that define the state of each map adopt the same value for all the coupled maps at each time step t, i.e., $x_t^{(1)} = x_t^{(2)} = \cdots = x_t^{(N)} \equiv x_t^{(*)}$. One can easily check that this state is a solution of Eq. (1). Geometrically, this condition defines a one-dimensional synchronization manifold (SM) embedded in the full N-dimensional phase space of the system. Its stability with respect to small perturbations in directions transversal to the SM can be determined from the analysis of the asymptotic Lyapunov spectrum (LS) calculated in synchronous states. As far as the completely synchronized (CS) state stays in the direction associated to the largest exponent, it will be transversely stable if the second largest Lyapunov exponent (and together with it the remaining ones) is negative [6,7]. Limitations of this linear stability criterion are

* Corresponding author. Tel.: +55 21 22363060.
E-mail address: celia@cbpf.br (C. Anteneodo).

0167-2789/$ - see front matter © 2006 Published by Elsevier B.V.
doi:10.1016/j.physd.2006.10.001

discussed in Ref. [8]. However, for a wide class of chaotic maps (including the logistic map) [8], the criterion of negativity of the second largest Lyapunov exponent evaluated in the CS state is appropriate and allows us to find a *synchronization domain* in parameter space, for which the CS state is asymptotically attained (see also [9]). Explicit results have been reported before for algebraically decaying interactions [2,3] and for uniform interactions with a cut-off distance [4]. Inside the synchronization domain, CS eventually occurs after a transient whose typical duration diverges as one approaches the critical frontier. Close outside that domain, intermittent behavior between laminar, quiescent states of synchronized behavior, and irregular bursting may occur.

In this paper, we will focus on CMLs whose local dynamics is ruled by the logistic map $x \mapsto 4x(1-x)$. In numerical examples we will restrict to the regular coupling scheme given by (1), where $B(r)$ decays algebraically with distance, while analytical considerations apply to more general definitions of $B(r)$. For these extended systems, we will discuss details of the synchronization transition, such as relaxation to the CS state and intermittent behavior, under the light of the statistics of largest transversal finite-time Lyapunov exponents (LTFEs). We will emphasize the consequences that the particular statistics of LTFEs at the Ulam point has on the relaxational dynamics in the vicinity of the synchronization transition.

2. Finite-time Lyapunov spectrum in synchronous states

Let us recall in this section some definitions and results that, although essentially already known, will be cited in the paper. Following standard calculations for the determination of Lyapunov exponents [10], by differentiating Eq. (1), the evolution of tangent vectors $\xi = \delta\mathbf{x}$ is given by $\xi_{t+1} = \mathbf{T}_t\xi_t$, where the Jacobian matrix $\mathbf{T}_t$ is

$$\mathbf{T}_t = \left(1 - \varepsilon + \frac{\varepsilon}{\eta}\mathbf{B}\right)\mathbf{D}_t \equiv \hat{\mathbf{B}}\mathbf{D}_t, \tag{2}$$

with the matrices $\mathbf{D}_t$ and $\mathbf{B}$ defined, respectively, by $D_t^{ij} = \delta_{ij} f'(x_t^{(i)})$ and $B_{ij} = [1-\delta_{ij}]B(r_{ij})$, being $r_{ij} = \min_{k\in\mathcal{Z}} |i - j + kN|$. The evolution of a given initial tangent vector ξ_0, after a time interval of length n, is $\xi_n = \mathcal{T}_n\xi_0$, where $\mathcal{T}_n \equiv \mathbf{T}_{n-1}\ldots\mathbf{T}_1\mathbf{T}_0$. Finite-time exponents (FEs) over that interval are obtained as $\lambda_k(n) = \ln \Lambda_n^{(k)}$, for $k = 1,\ldots,N$, where $\{\Lambda_n^{(k)}\}$ are the eigenvalues of $\hat{\Lambda}_n = (\mathcal{T}_n^T\mathcal{T}_n)^{\frac{1}{2n}}$ [10].

In the CS state, the dynamical variables of all maps at each time step t have the same value $x_t^{(*)}$. In this case, $\mathbf{D}_t = f'(x_t^{(*)})\mathbb{1}_N$, thus, $\mathbf{T}_t = f'(x_t^{(*)})\hat{\mathbf{B}}$ and $\mathcal{T}_t^T\mathcal{T}_t = (\prod_{j=0}^{t-1}[f'(x_j^{(*)})]^2)\hat{\mathbf{B}}^{2t}$. Therefore, the spectrum of FEs over a time interval of length n in the CS state (that we shall denote with the superindex "s") is given by:

$$\lambda_k^s(n) = \frac{1}{n}\sum_{i=0}^{n-1}\ln|f'(x_i^{(*)})| + c_k, \quad k = 1,\ldots,N, \tag{3}$$

with $c_k \equiv \ln|1 - \varepsilon + \varepsilon b_k/\eta|$, where b_k, the eigenvalues of the interaction matrix $\mathbf{B}$, are given by $b_k = 2\sum_{m=1}^{N'} B(m)\cos(2\pi km/N)$, for odd N. Here $x_i^{(*)} = f^i(x_0^{(*)})$ is the ith iterate of the initial state $x_0^{(*)}$, the same for the N maps, since we are evaluating the exponents in CS states.

In the asymptotic case $n \to \infty$, and assuming ergodicity, the first term in the right-hand side of Eq. (3), which represents a time average, can be substituted by an ensemble average over the single-map attractor. In such a case one gets the asymptotic LS

$$\lambda_k^s = \lambda_U + c_k, \tag{4}$$

where $\lambda_U = \langle\ln|f'(x^{(*)})|\rangle$ is the Lyapunov exponent of the uncoupled map. Notice that the parameters that define the particular uncoupled map affect only λ_U, while $\{c_k\}$ are determined by the particular cyclic dependence on distance in the regular coupling scheme. As discussed above, the negativity of the second largest (or largest transversal) asymptotic exponent $\lambda_\perp^s$ allows us to delimit the synchronization domain. For the particular interaction iterations, the domain is bounded by [2,3] (see also [11])

$$\frac{1-\mathrm{e}^{-\lambda_U}}{1-b_1/\eta} < \varepsilon < \frac{1+\mathrm{e}^{-\lambda_U}}{1-b_{N'}/\eta}, \tag{5}$$

where $b_k = 2\sum_{m=1}^{N'}\cos(2\pi km/N)/m^\alpha$, for odd N.

Unlike infinite-time exponents, finite-time ones strongly depend on the initial conditions. Starting from random $x_0^{(*)}$, the fluctuations in the values of $\lambda_k^s(n)$ arise from the summation in (3) only. As a consequence, all the $\lambda_k^s(n)$ of the spectrum have a probability density function (PDF) with the same shape, differing only in the mean value $\langle\lambda_k^s(n)\rangle = \lambda_U + c_k$, which typically coincides with the infinite-time exponent λ_k^s. While the average of $\lambda_k^s(n)$ depends on the lattice parameters embodied in c_k, its variance does not, it is only determined by the local features of the single map. In fact, when CS is attained, all maps evolve with the dynamics of an uncoupled map, then the PDFs of FEs for the whole array are straightforwardly obtained from the PDF of FEs of the local map by simply shifting the mean value.

For the logistic map $x \mapsto 4x(1-x)$, the PDF of the one-step ($n = 1$) FE can be calculated from the invariant measure of the Ulam attractor [12]. It is

$$P(\lambda(1)) = \frac{2}{\pi}\frac{1}{\sqrt{4\mathrm{e}^{-2[\lambda(1)-\lambda]}-1}}, \tag{6}$$

for $\lambda(1) - \lambda < \ln 2$, and zero otherwise, where $\lambda = \ln 2$ is the asymptotic value.

For large enough n, a smooth approximate expression for the PDF of FEs is given by [13]

$$P(\lambda(n)) \simeq \frac{2n}{\pi^2}\ln(\coth|n[\lambda(n)-\lambda]/2|). \tag{7}$$

For $\lambda(n) < \lambda$, expression (7) is exact, however, for $\lambda(n) > \lambda$, the exact PDF presents a complex structure with 2^{n-1} spikes that get narrower and accumulate close to the mean value with increasing n [12,13]. Therefore, in the latter interval, expression (7) constitutes a smooth approximation, such that the sharp

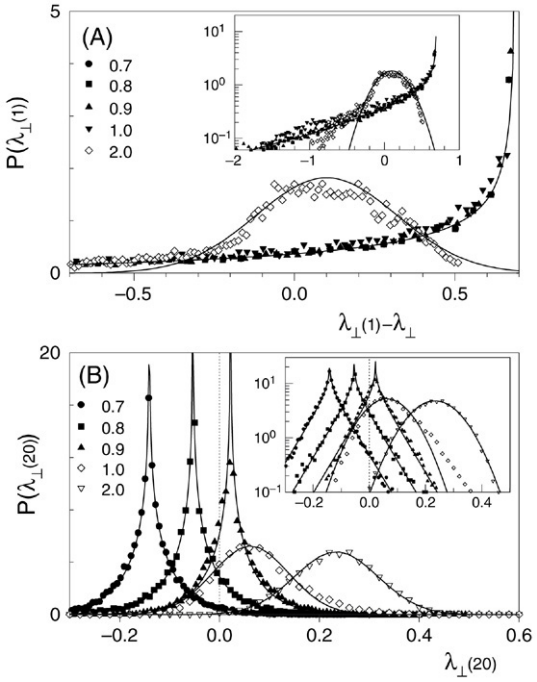

Fig. 1. Comparison between numerical and theoretical PDFs. They correspond to the largest transversal one step (A) and time-20 (B) exponents of $N = 21$ coupled logistic maps, with algebraically decaying interactions, for $\varepsilon = 0.8$ and different values of α (above $\alpha_c \simeq 0.867$, stability of the CS state is lost). Numerical PDFs are represented by symbols. Solid lines associated to full symbols correspond to the theoretical predictions for synchronous states, while those associated to hollow symbols correspond to Gaussian fittings. Inset: semi-log representation to exhibit the tails.

spikes have been trimmed by finite size bins. Moreover, the exact PDF is non-null only for $\lambda(n) - \lambda \leq \ln 2$.

Even the smooth PDF (7) is markedly different from Gaussian. It is divergent at $\lambda(n) = \lambda$ and falls off with exponential tails. It is noteworthy that the variance decays anomalously as $1/n^2$ [13,14]

$$\sigma^2(n) = \frac{\pi^2}{6n^2}\left(1 - \frac{1}{2^n}\right), \tag{8}$$

instead of the usual $1/n$ decay. Also notice that the PDFs (7) for different values of n would collapse into a single shape via rescaling by n.

3. Distribution of finite-time Lyapunov exponents

Fig. 1 exhibits numerical PDFs for CMLs together with the analytical predictions for synchronous states. Numerical PDFs were built by choosing 10^4 initial conditions and computing the second eigenvalue of the matrix $\hat{\Lambda}_n$ after a transient. Eqs. (6) and (7), for single maps, are in excellent agreement with numerical PDFs for LTFEs, within parameter ranges yielding coherent states, as expected. We also note that analytical expressions (6) and (7) still allow us to describe numerical distributions of transversal exponents even close outside the synchronization domain. Although we have chosen to display scans of the synchronization threshold at fixed ϵ (at the intermediate value $\epsilon = 0.8$), the results exhibited are

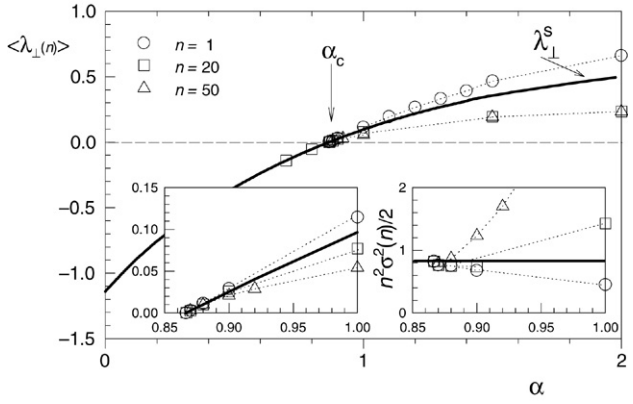

Fig. 2. Average n-step exponents as a function of α for the same CML of Fig. 1. Left side inset: zoom around critical values. Right side inset: scaled standard deviation. In all cases full lines correspond to the asymptotic value in synchronous states.

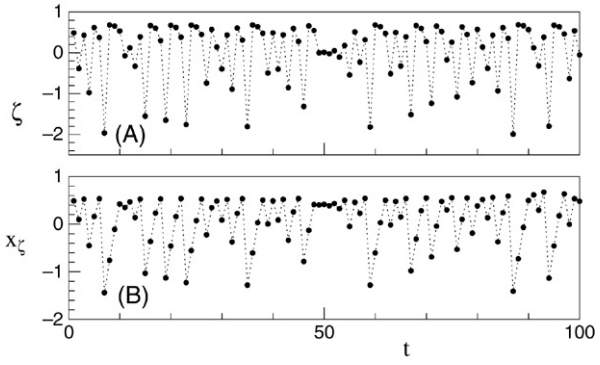

Fig. 3. Time evolution of $\zeta = \lambda_\perp(1) - \lambda_\perp$ (A) and $x_\zeta = \sum_{t=1}^{t} \zeta(t)$ (B) for the same CML of Fig. 1 with $\alpha = 0.9$ (supercritical).

representative of those observed for other values of ϵ as well as for other directions across the frontier.

In Fig. 2 we display the average and standard deviation of LTFEs. In fact, average values remain close to the theoretical estimate in CS states up to $\alpha - \alpha_c \simeq 0.15$. However, the dispersion of the data deviates from CS estimates as n increases, which indicates that the theoretical PDF for synchronous states is not expected to be a good approximation for very large n outside the synchronization domain. The fact that theoretical estimates obtained for synchronous states also hold close outside the threshold means that, despite the noise introduced by the "bath" of coupled maps, correlations persist in that region spoiling Gaussianity. Whereas, far enough from the threshold ($\alpha > 1$), correlations can be neglected and Gaussian shapes arise (Fig. 1).

To illustrate the temporal evolution of centered one-step exponent $\zeta = \lambda_\perp(1) - \lambda_\perp$, a time series is displayed in Fig. 3 for supercritical α ($\alpha = 0.9$). Similar antipersistent fluctuations also occur for uncoupled maps, hence, also for CMLS with subcritical α, in accord with the distributions exhibited in Fig. 1(A). Notice, in Fig. 3, the non-diffusive character of the random walk associated to successive steps ζ, consistently with the expression for the variance in Eq. (8).

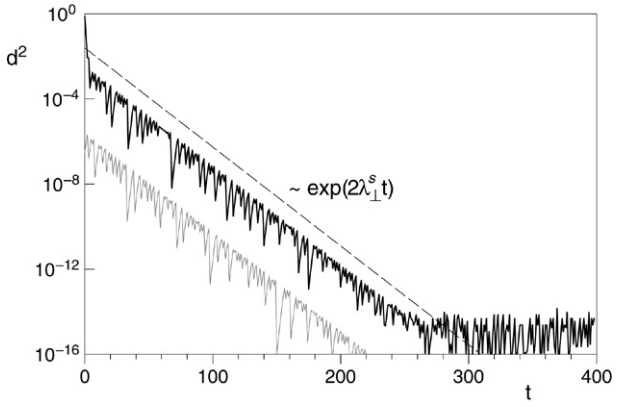

Fig. 4. Relaxation to the synchronization manifold. Time series of d^2 for the same CML of Fig. 1 with $\alpha = 0.8$ (subcritical). The dashed line corresponds to the exponential law indicated in the figure, for comparison. The gray line corresponds to a realization of Eq. (10).

4. Implications of fluctuating exponents

4.1. Subcritical regime

For parameter values belonging to the synchronization domain, that is, for subcritical α, all other parameters kept fixed, the system eventually converges to the CS state. In fact, asymptotically, the CS states is stable since the PDF of LTFEs collapses to a Dirac delta function centered at $\lambda^s_\perp$, which is negative in that domain. The relaxation to the CS state can be measured, for instance, by means of either the distance to the SM, defined through $d(t) = \sqrt{\sum_i (x_t^{(i)} - \langle x_t \rangle)^2}$, or the order parameter $R(t) = |\sum_i \exp(2\pi x_t^{(i)})|/N$. Since, for small deviations from the SM, both quantities are related through $d^2 \simeq (1 - R^2)/2$, we will exhibit the time evolution of d^2 only. After a very brief transient, the decay to the CS state is exponential with a characteristic time given by $\tau_c = 1/|\lambda^s_\perp|$ (see Fig. 4), that diverges at the critical frontier. For the power-law interaction, $\lambda^s_\perp$ scales as $|\lambda^s_\perp| \sim |\alpha - \alpha_c|$ and $|\lambda^s_\perp| \sim |\varepsilon - \varepsilon_c|$, at the critical point.

The fact that the PDF of LTFEs spreads over negative and positive values (Fig. 1), once assumed stationarity has been attained (e.g., Fig. 3), implies that the exponents, computed over finite-time segments of a trajectory, fluctuate around zero. On the one hand, as one approaches the frontier subcritically, the mean value of the distribution shifts to zero from negative values. On the other hand, as one follows a trajectory for a longer time interval, the PDF of LTFEs concentrates around the mean. Then, there may be segments of trajectory which are repelled from the SM. But, on average, trajectories are attracted to the SM exponentially fast. Due to the finite precision of computer calculations, the distance to the SM saturates at a non-null value (see d^2 vs t in Fig. 4 for $t > 300$). Intrinsic noise, due to numerical truncation, may drive the state of the system slightly away from the saturation level. However, each time this happens, the distance decays, again exponentially fast, to its lower bound. This is a scenario generically observed, whereas we want to focus on the specific features that arise due to the local dynamics here considered.

The decay to the SM in the subcritical regime, illustrated in Fig. 4, can be suitably described by considering that in first approximation

$$d(t) = \exp[\lambda^s_\perp(1)]d(t-1), \tag{9}$$

which leads to

$$d(t) = d_o \exp\left[\lambda^s_\perp t + \sum_{i=1}^{t} \zeta(i)\right] = d_o \exp[\lambda^s_\perp(t)t], \tag{10}$$

where the fluctuating component $\zeta = \lambda^s_\perp(1) - \lambda^s_\perp$ corresponds to successive centered one-step LTFEs, according to Eqs. (3) and (4). As discussed in Section 3, the distribution of $\lambda^s_\perp(1)$ in synchronized states follows that of one-step FEs in the uncoupled map, given by Eq. (6), therefore $P(\zeta) = \frac{2}{\pi}\frac{1}{\sqrt{4e^{-2\zeta}-1}}$, with $\zeta \in (-\infty, \ln 2)$. Notice that ζ, with zero mean, is bounded from above. This explains the upper bound of the fluctuations superposed to the exponential decay in Fig. 4. In fact, the fluctuations around the exponential envelope can be fully described by the statistics of time-one exponents according to Eq. (10), as illustrated in Fig. 4 (gray line).

Breakdown of shadowability might occur, as exponents fluctuating about zero are a signature of unstable dimension variability (UDV) [15]. UDV occurs when the unstable periodic orbits embedded in the chaotic invariant set have different numbers of unstable directions [16]. A consequence is the breakdown of shadowability for typical chaotic trajectories [17]. A true chaotic trajectory is said to be *continuously shadowable* if there exists another chaotic trajectory which: (i) stays close to the former one for a sufficiently long time, and (ii) may be continuously deformable to the chaotic trajectory [18]. In this case, noisy chaotic trajectories of a dynamical system, such as those produced by numerical integration, are continuously shadowed by true ones [19]. Continuous shadowability, however, cannot be always taken for granted in chaotic systems. For the special case of hyperbolic systems, this mathematical property holds for an infinite time [20], but the majority of dynamical systems likely to be found in physical applications is non-hyperbolic.

Taking into account that the PDF of n-time exponents is null for $\lambda^s_\perp(n) \geq \lambda^s_\perp + \ln 2$ [12,13], then if $\lambda^s_\perp(\alpha, \varepsilon, N) < -\ln 2$, the finite-time exponents are negative for almost any initial condition. Thus, this point would correspond to the onset of shadowability. Whereas, for $-\ln 2 < \lambda^s_\perp$, although the mean of the distribution may be negative, there is always a non-null fraction φ of positive exponents given by $\varphi = \int_0^\infty \mathrm{d}\lambda^s_\perp(n) P(\lambda^s_\perp(n))$, pointing to the possibility of loss of shadowability of numerical trajectories [21]. Because φ grows from zero with a very small slope, since the positive tail of the PDF is approximately exponential, then the onset may appear shifted towards the threshold in numerical computations [22].

4.2. Supercritical regime

For supercritical α, that is outside the synchronization domain, the CS state is not asymptotically stable, because $\lambda^s_\perp > 0$. Fig. 5 shows that, close enough to the boundary,

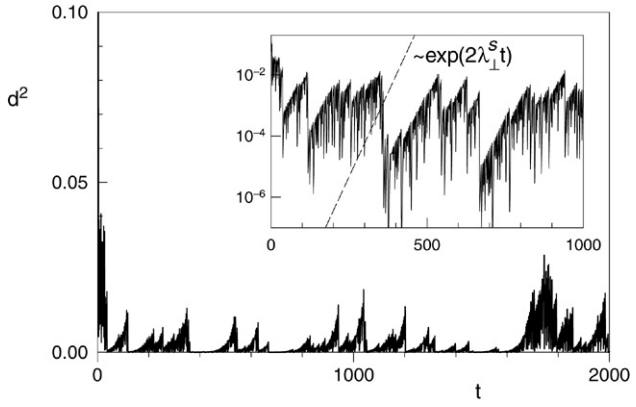

Fig. 5. Time series of d^2 for the same CML of Fig. 1 with $\alpha \simeq 0.9$ (supercritical). Inset: semi-log representation of the same data. The dashed line corresponds to the exponential law indicated in the figure, for comparison.

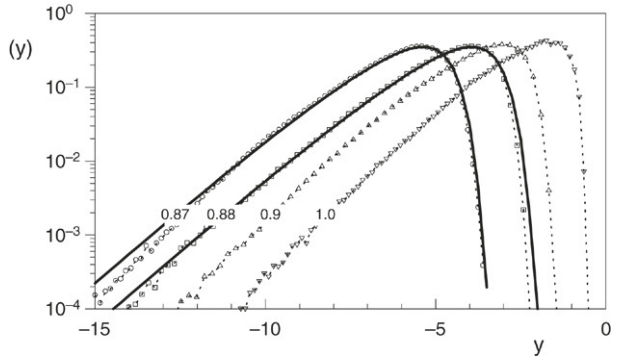

Fig. 6. Distribution of the logarithmic distance $y = \ln d$, for the same CML of Fig. 1 ($N = 21$) and different supercritical values of α. For comparison, full lines correspond to the analytic distribution for $N = 2$ given by Eq. (11) with $\delta = 2(\alpha - \alpha_c)$.

a succession of correlated bursts away from the SM occur. Although this figure exhibits a time series up to $t = 2000$, the same features are observed for longer runs (typically performed up to $t = 10^7$). Close to the instability threshold (up to $\alpha \simeq 0.9$ for $\epsilon = 0.8$), the numerical estimate for $\lambda_\perp$ fairly coincides with $\lambda_\perp^s$ (as shown in Fig. 2) and the PDF of LTFEs can be described by Eq. (7). Although the average $\langle \lambda_\perp^s(n) \rangle = \lambda_\perp^s$ is positive, there is a non-null probability that the LTFE be negative, thus leading to intermittent behavior at finite times. Then there are time intervals during which the trajectories are either attracted to or repelled on average from the SM. Naturally, the average duration of the time intervals in which the array is synchronized increases when approaching the synchronization threshold; however, synchronization is not attained as a final stable state.

This is a quite general scenario for intermittency. For the particular local dynamics considered here, intermittent bursts are asymmetrical. There is an exponential growth with a characteristic time given by $1/\lambda_\perp^s$ (see inset of Fig. 5) that has the same scaling laws as the subcritical characteristic time. After each non-regular time interval of exponential growth, the distance to the SM falls down abruptly. It fluctuates around a reference level ($\langle d \rangle \simeq 0.037$ for the parameters in Fig. 5) that increases with α. The peculiar intermittent dynamics can be understood in terms of the statistics of LTFEs. In the supercritical regime Eq. (10) constitutes a very crude approximation, since nonlinearities are expected to be crucial in this case. However, it explains the local exponential growth with exponent $1/\lambda_\perp^s > 0$, as well as the superposed upper bounded fluctuations. As d increases, nonlinearities become dominant and they are responsible for the sharp drops. This nonlinear effect has been analyzed in detail before for two coupled logistic maps [23,24].

Close to the threshold, the average distance increases linearly with $\lambda_\perp^s \sim |\alpha - \alpha_c|$. Also, for increasing α, the correlated bursts become more frequent (hence, its duration becomes shorter) such that far from the frontier fluctuations decorrelate and the intermittent clustering effect disappears. Moreover, in that region, the numerical estimate of $\lambda_\perp$ significantly deviates from the one calculated for synchronous states and new features, outside the scope of the present work, may occur.

Histograms of logarithmic distances $y \equiv \ln d$ (directly built for y) are presented in Fig. 6. They initially grow approximately as $\exp(y)$, and above the maximum value fall off faster than exponentially. For two coupled logistic maps ($N = 2$), an analytical expression can be obtained as the marginal density of the joint probability derived in Ref. [23]:

$$Q(y) = \frac{4e^y}{\pi^2 \delta} \int_0^1 \frac{dx}{1-x^2} \exp\left(-\frac{1}{\pi \delta^2} \frac{e^{2y}}{1-x^2}\right), \tag{11}$$

for small enough $\delta \propto (\alpha - \alpha_c)$. This theoretical PDF is also plotted in Fig. 6 (with $\delta \propto \lambda_\perp^s \propto |\alpha - \alpha_c|$) for comparison. Notice that the analytic distribution derived for two coupled logistic maps is in agreement with the corresponding histogram $P(y)$ for a larger lattice, in the vicinity of the transition. $P(y)$ is also connected with the distribution of synchronization times discussed in Ref. [8]. Let us also note that for large negative y, $P(y)$ behaves as $\exp(y)$, instead of $\exp(hy)$, with $h = 2\lambda_\perp/\sigma_1^2$ (hyperbolicity exponent), derived under the assumption of Gaussian fluctuations [25].

A universal result is that, at the onset of intermittency, the distribution of laminar phases (inter-burst time intervals) of length τ decays as $\tau^{-\beta}$ [7,26–28], meaning the presence of lengths of arbitrarily large size. In particular the size of the average plateau diverges. Moving far from the onset, the tail of the distribution of laminar phases is gradually dominated by an exponential decay. In general, the distribution of laminar phases can be obtained by solving a first-return problem, that, for white Gaussian noise, yields the exponent $\beta = 3/2$ [7,26]. However, as we have seen, in our case, close to the threshold, the distribution of finite-time exponents deviates from the Gaussian approximation. Therefore, deviations from the 3/2 power law decay are also expected [28]. We measured inter-burst sizes, that is, the length of time segments during which the distance d remains below a threshold value d_o. Numerical distributions of inter-burst sizes are displayed in Fig. 7 for different values of (α, ϵ) close outside the synchronization domain. Histograms were built by computing the number of occurrences of each (integer) value of τ over runs of at least 10^8 steps. A threshold value $d_o \simeq 2\langle d \rangle$ was used, but the decay

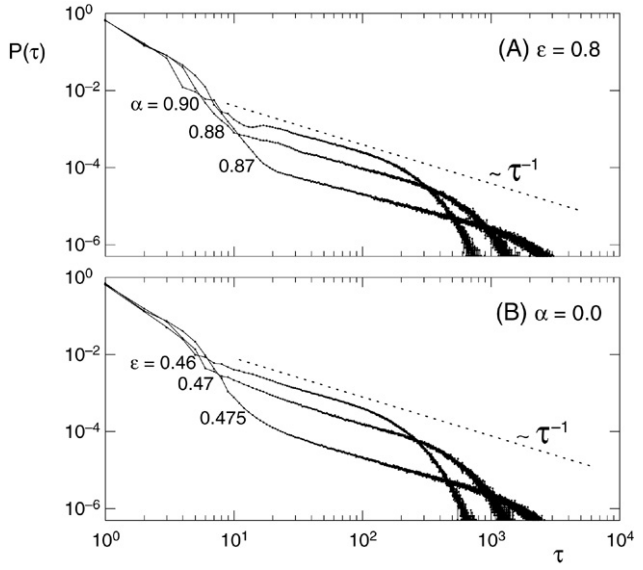

Fig. 7. Distributions of inter-burst times for CMLs with $N = 21$ and different values of lattice parameters (α, ϵ) indicated on the graph. In (A) $\epsilon = 0.8$ is fixed and $\alpha_c \simeq 0.867$, in (B) $\alpha = 0.0$ is fixed and $\epsilon_c \simeq 0.476$. Histograms were accumulated over at least 10^8 iterations. In all cases, $d_o \simeq 2\langle d \rangle$. Dotted lines, corresponding to the power law with exponent $\beta = 1$, were drawn for comparison.

laws do not substantially depend on the choice of the threshold d_o. In general, one observes a rapid decay for very small τ, an intermediate region with a decay that can be approximated by a power law with $\beta \simeq 1$ ($\beta = 0.95 \pm 0.06$) and finally, for large enough τ, a cross-over to an asymptotic exponential decay. The observed decay is at neat variance with the power-law decay with $\beta = 3/2$. In fact, depending on the type of correlations, different exponents may arise [28]. In particular, some subdiffusive processes characterized by the variance of the diffusive variable evolving as t^γ with $0 < \gamma < 1$ may yield distributions of first return times characterized by $\beta = 1 + \gamma/2$. Recall that time-one exponents present antipersistence and yield non-diffusive random walks ($\gamma = 0$). Although $\beta = 1$ may arise in the limit $\gamma \to 0$, logarithmic corrections, hardly detectable numerically, are also expected.

5. Concluding remarks

We have investigated the synchronization threshold of coupled logistic maps. We have analyzed details of diverse phenomena occurring close to the SM, such as relaxation and bursting behavior, through the statistical properties of finite-time Lyapunov exponents for single maps. Moreover, we have included comparisons of our results for extended systems with previous ones in the literature for single and two coupled maps. From this perspective, we have exhibited peculiar features appearing when dealing with coupled logistic maps at the Ulam point. This particular behavior was connected to the non-Gaussian character of fluctuations in the vicinity of the synchronization threshold. These issues are particularly important since the logistic map is commonly used as a paradigm of chaotic systems. Although experiments were performed for CMLs with interactions decaying with distance as a power law, most of our results are expected to be valid for more general coupling schemes as soon as the same local dynamics is considered.

Acknowledgments

This work was partially supported by Brazilian agencies CAPES, CNPq and Fundação Araucária.

References

[1] K. Kaneko, in: K. Kaneko (Ed.), Theory and Applications of Coupled Map Lattices, Wiley, Chichester, 1993.
[2] C. Anteneodo, S.E. de S. Pinto, A.M. Batista, R.L. Viana, Phys. Rev. E 68 (2003) 045202(R);
C. Anteneodo, S.E. de S. Pinto, A.M. Batista, R.L. Viana, Phys. Rev. E 69 (2003) 029904(E).
[3] C. Anteneodo, A.M. Batista, R.L. Viana, Phys. Lett. A 326 (2004) 227.
[4] P.G. Lind, J. Corte-Real, J.A.C. Gallas, Phys. Rev. E 69 (2004) 026209.
[5] A. Pikovsky, M. Rosenblum, J. Kurths, S. Strogatz, Synchronization: A Universal Concept in Nonlinear Sciences, CUP, Cambridge, 2001;
S. Boccaletti, J. Kurths, G. Osipov, D.L. Valladares, C.S. Zhou, Phys. Rep. 366 (2002) 1.
[6] P.M. Gade, C.-K. Hu, Phys. Rev. E 60 (1999) 4966;
P.M. Gade, H.A. Cerdeira, R. Ramaswamy, Phys. Rev. E 52 (1995) 2478.
[7] M. Ding, W. Yang, Phys. Rev. E 56 (1997) 4009.
[8] M. Cencini, A. Torcini, Physica D 208 (2005) 191.
[9] L.M. Pecora, T.L. Carrol, Phys. Rev. Lett. 80 (1998) 2109.
[10] J.-P. Eckmann, D. Ruelle, Rev. Modern Phys. 57 (1985) 617.
[11] P.G. Lind, J.A.C. Gallas, H.J. Herrmann, in: M. Ausloos, M. Dirickx (Eds.), The Logistic Map and the Route to Chaos: From the Beginnings to Modern Applications, Springer, Heidelberg, 2005.
[12] A. Prasad, R. Ramaswamy, Phys. Rev. E 60 (1999) 2761.
[13] C. Anteneodo, Phys. Rev. E 69 (2004) 016207.
[14] J. Theiler, L.A. Smith, Phys. Rev. E 51 (1995) 3738.
[15] S.P. Dawson, C. Grebogi, T. Sauer, J.A. Yorke, Phys. Rev. Lett. 73 (1994) 1927.
[16] R. Abraham, S. Smale, Proc. Sympos. Pure Math. (AMS) 14 (1970) 5;
F.J. Romeiras, C. Grebogi, E. Ott, W.P. Dayawansa, Physica D 58 (1992) 165.
[17] Y.-C. Lai, C. Grebogi, J. Kurths, Phys. Rev. E 59 (1999) 2907;
S.P. Dawson, Phys. Rev. Lett. 76 (1996) 4348;
Y.-C. Lai, Phys. Rev. E 59 (1999) R3807;
E. Barreto, P. So, Phys. Rev. Lett. 85 (2000) 2490;
R. Davidchack, Y.-C. Lai, Phys. Lett. A 270 (2000) 308.
[18] C. Grebogi, L. Poon, T. Sauer, J.A. Yorke, D. Auerbach, in: B. Fiedler (Ed.), Handbook of Dynamical Systems, vol. 2, Elsevier Science, 2002.
[19] C. Grebogi, S. Hammel, J.A. Yorke, J. Complexity 3 (1987) 136; Bull. Amer. Math. Soc. 19 (1988) 465.
[20] D.V. Anosov, Proc. Steklov Inst. Math. 90 (1967) 1;
R. Bowen, J. Differential Equations 18 (1975) 333.
[21] R.L. Viana, S.E. de S. Pinto, J.R.R. Barbosa, C. Grebogi, Internat. J. Bifur. Chaos 13 (2003) 3235.
[22] R.L. Viana, C. Grebogi, S.E. de S. Pinto, S.R. Lopes, A.M. Batista, J. Kurths, Phys. Rev. E 68 (2003).
[23] S.P. Kuznetsov, A.S. Pikovsky, Radiofizika 32 (1989) 49.
[24] Yu.L. Maistrenko, V.L. Maistrenko, A. Popovych, E. Mosekilde, Phys. Rev. Lett. 80 (1998) 1638; Phys. Rev. E 60 (1999) 2817.
[25] S.C. Venkataramani, T.M. Antonsen Jr., E. Ott, J.C. Sommerer, Physica D 96 (1996) 66.
[26] N. Platt, E.A. Spiegel, C. Tresser, Phys. Rev. Lett. 70 (1993) 279;
J.F. Heagy, N. Platt, S.M. Hammel, Phys. Rev. E 49 (1994) 1140;
H.L. Yang, E.J. Ding, Phys. Rev. E 54 (1996) 1361.
[27] A. Čenys, A. Namajūnas, A. Tamaševičius, T. Scheneider, Phys. Lett. A 213 (1996) 259;
M. Sauer, F. Kaiser, Phys. Lett. A 243 (1998) 38.
[28] M. Ding, W. Yang, Phys. Rev. E 52 (1995) 207;
G. Rangarajan, M. Ding, Phys. Lett. A 273 (2000) 322.